

Controlled insertion and retrieval of atoms coupled to a high-finesse optical resonator

M Khudaverdyan¹, W Alt, I Dotsenko², T Kampschulte, K Lenhard, A Rauschenbeutel³, S Reick, K Schörner, A Widera and D Meschede

Institut für Angewandte Physik, Universität Bonn,
Wegelerstr. 8, 53115 Bonn, Germany
E-mail: mika@iap.uni-bonn.de

New Journal of Physics **10** (2008) 073023 (16pp)

Received 6 May 2008

Published 11 July 2008

Online at <http://www.njp.org/>

doi:10.1088/1367-2630/10/7/073023

Abstract. We experimentally investigate the interaction between one and two atoms and the field of a high-finesse optical resonator. Laser-cooled caesium atoms are transported into the cavity using an optical dipole trap. We monitor the interaction dynamics of a single atom strongly coupled to the resonator mode for several hundred milliseconds by observing the cavity transmission. Moreover, we investigate the position-dependent coupling of one and two atoms by shuttling them through the cavity mode. We demonstrate an alternative method, which suppresses heating effects, to analyse the atom–field interaction by retrieving the atom from the cavity and by measuring its final state.

¹ Author to whom any correspondence should be addressed.

² Present address: Laboratoire Kastler Brossel, Ecole Normale Supérieure et Collège de France, 24 rue Lhomond, 75231 Paris Cedex 05, France.

³ Present address: Institut für Physik, Johannes Gutenberg-Universität, Staudingerweg 7, 55099 Mainz, Germany.

Contents

1. Introduction	2
2. Experimental apparatus	3
2.1. Trapping and transporting single atoms	3
2.2. High-finesse cavity	4
3. Strong coupling of a single atom to the resonator mode	8
3.1. Coupling to the centre of the mode	8
3.2. Position-dependent coupling	11
4. Coupling of one and two atoms	12
5. Detection of the final atomic state	13
6. Summary and outlook	15
Acknowledgments	16
References	16

1. Introduction

Single neutral atoms have been shown to be excellent carriers of quantum information [1]. A great challenge and a key requirement for the utilization of these systems, e.g. the construction of multi-particle entangled states, is the realization of controlled coherent interactions between two or more individual atoms. The intriguing properties of such systems may lead to advances in the fields of quantum information processing and quantum simulation [2].

One possible realization of a well-controlled interaction is to couple trapped atoms to the light field of a high-finesse optical resonator [3], thereby mediating an interaction between the atoms [4, 5]. Coupled atom–cavity systems in the optical domain have been investigated in several recent experiments [6, 7], including deterministic insertion of the atoms into the cavity field [8]. In all cases the information about the atom–light interaction has been inferred from the light field. In contrast, in our work we use deterministic coupling of a single or few atoms to a high-finesse optical cavity and extract complementary information about the atom–light interaction from both the light leaking from the cavity and the internal atomic state.

In our experiment, we prepare laser-cooled atoms inside a standing wave dipole trap and deterministically transport them to a pre-defined position inside the mode of a high-finesse optical resonator, see figure 1. Due to the strong atom–cavity interaction, even a single atom causes a well-known dramatic drop of the observed transmission of a resonant laser beam (‘probe laser’) through the cavity [7, 9]. By slowly transporting one or two atoms through the cavity mode, we map out the spatial variation of the cavity field. In the experiment with two atoms, we detect an increased effective coupling compared to the case of a single atom.

Complementing these purely optical measurements, we read out the final hyperfine state of the atom after its interaction with the cavity, and thereby we obtain information in a different way. Thus, we pave the way for the detection of entangled or correlated multi-atom states.

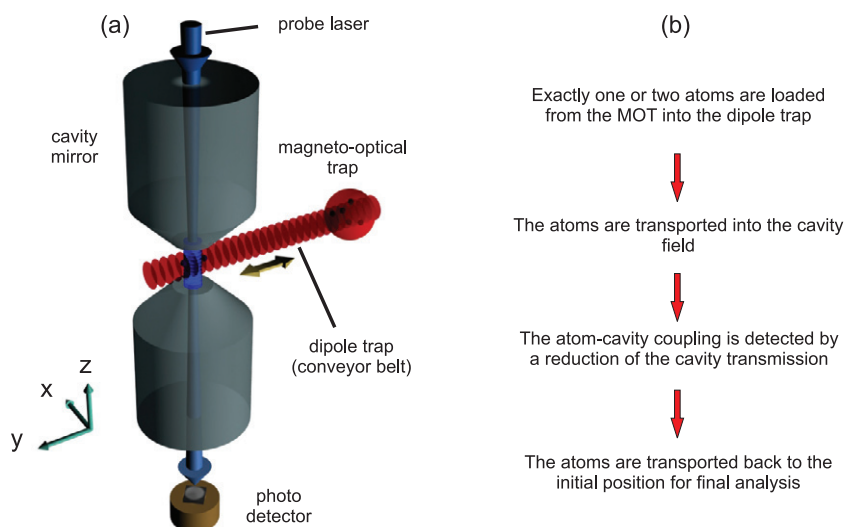


Figure 1. Concept of the experiment: (a) schematic drawing of the experiment and (b) outline of the basic experimental procedure.

2. Experimental apparatus

2.1. Trapping and transporting single atoms

We use a high-gradient magneto-optical trap (MOT) operating inside an ultra-high vacuum glass cell as a source of cold caesium atoms, see figure 2. The small capture volume of the MOT allows us to cool and trap single or few atoms, which are detected by imaging their fluorescence both onto an intensified CCD camera and an avalanche photodiode (APD). From the fluorescence signal, we are able to deduce the number of trapped atoms within a few tens of milliseconds.

In order to prepare a predefined number of atoms between 1 and 10, we use a number-triggered loading technique [10]: the MOT is repeatedly and rapidly loaded until the desired number of atoms is detected, which are subsequently transferred without loss into the dipole trap.

The dipole trap is formed by interfering two counter-propagating laser beams with a wavelength of 1030 nm. Compared to free space transmission, a significant improvement in pointing stability and beam profile was obtained by using polarization-maintaining optical fibres with a large mode area (Passive-10/123-PM, LIEKKI) to guide the laser light from the source to the experimental setup, see figure 2. These improvements have led to a reduced scattering from the cavity mirrors, see section 2.2.3. The dipole trap laser beams with a total power of 2.9 W propagate through the MOT and are focused to a Gaussian beam radius of $w_0 = 34 \mu\text{m}$, located 1.7 mm away from the location of the MOT. At the position of the MOT, the beam radius is $w_{\text{MOT}} = 38 \mu\text{m}$ and the trap depth equals $k_B \times 0.58 \text{ mK}$. Both parameters are inferred from a measurement of the oscillation frequencies of the atoms in the trap using the experimental procedure described in [11]. The measured radial and axial oscillation frequencies of $\Omega_{\text{rad}}/2\pi = 1.6 \text{ kHz}$ and $\Omega_{\text{ax}}/2\pi = 262 \text{ kHz}$, respectively, agree within 10% with our calculations based on aberration-free, ideal Gaussian beams.

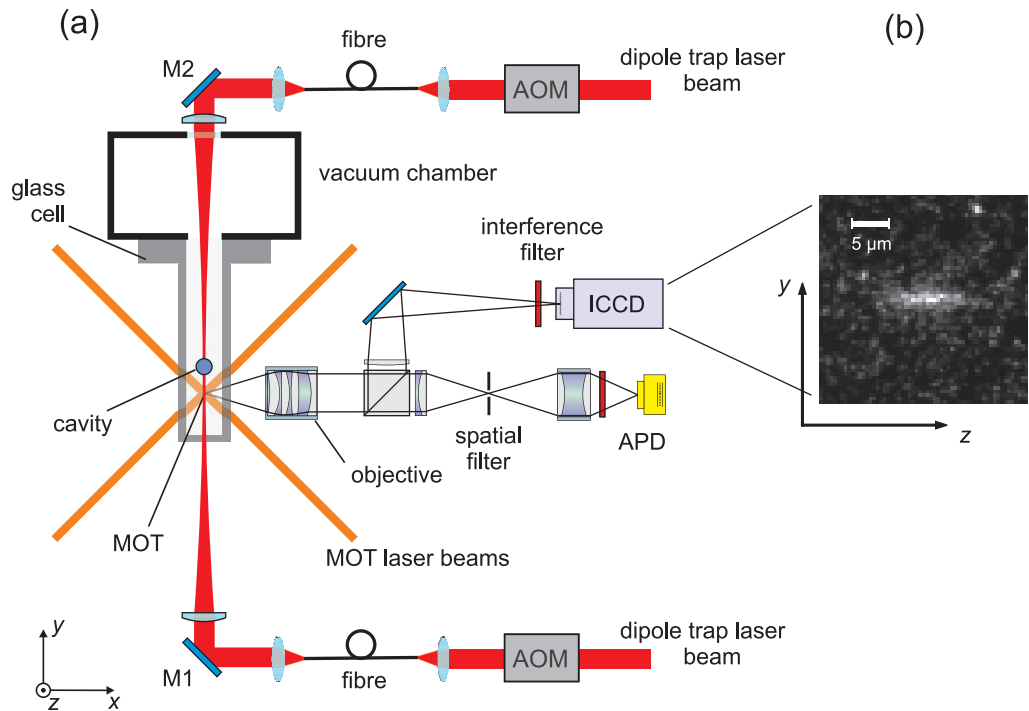


Figure 2. (a) Schematic view of the atom-trapping setup. Atoms are loaded from the MOT into the dipole trap and transported along the dipole trap axis into the cavity mode (oriented along the z -axis). The APD allows us to count trapped atoms and the ICCD camera provides information on their positions. (b) Fluorescence image of a single atom, illuminated for 1 s in the dipole trap.

In order to image atoms in the dipole trap, we illuminate them with three-dimensional optical molasses, tuned by several tens of megahertz to the red of the $|F = 4\rangle \rightarrow |F' = 5\rangle$ transition, providing both efficient Doppler cooling and continuous fluorescence. The position of individual atoms along the dipole trap axis is determined from the fluorescence image with an uncertainty of 140 nm [12]. The storage time of atoms in the dipole trap is up to several tens of seconds.

To transport the atoms along the dipole trap axis into the optical cavity, acousto-optic modulators (AOMs) are used as frequency shifters in both beams of the dipole trap. By mutually detuning their frequencies, we can set our standing wave into motion and use it as an optical conveyor belt. We transport atoms to the position of the cavity over about 5 mm within 4 ms with sub-micrometre precision [12].

2.2. High-finesse cavity

Our high-finesse optical cavity is composed of two concave mirrors consisting of highly reflective, multi-layer dielectric coatings on super-polished substrates (Research Electro-Optics). The glass substrates are 3 mm in diameter and are coned to 1 mm at the mirror surface, see figure 3. The reflectivity of each mirror is about 99.9997% at the Cs D_2 line (852 nm), resulting in a cavity finesse of $\mathcal{F} \approx 1 \times 10^6$. The transmission of the mirrors is $T = 1.3$ ppm and the losses due to absorption and scattering are about $A = 1.8$ ppm. A large atom-cavity

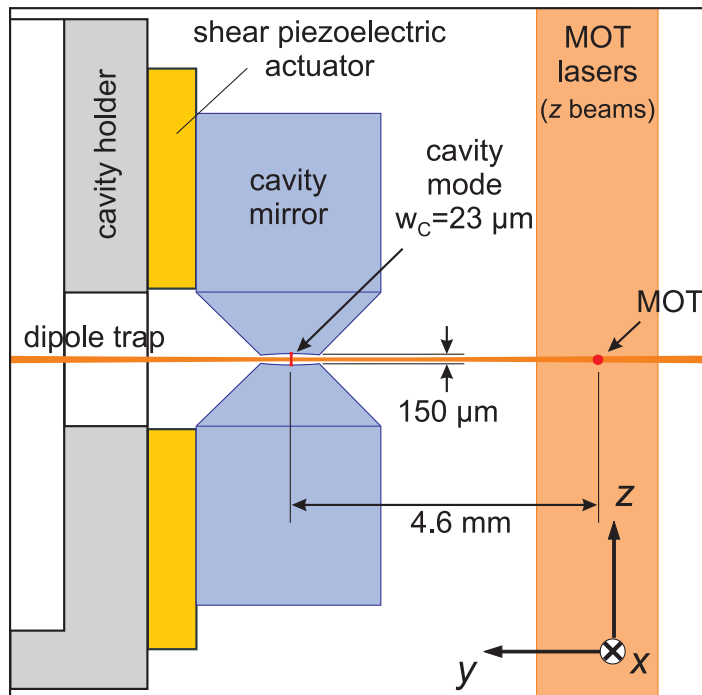


Figure 3. Schematic view of the high-finesse cavity integrated into our atom-trapping experiment. All elements, laser beams and their spatial separations are approximately drawn to scale.

coupling strength is achieved by realizing a small mode volume with two closely spaced mirrors. The separation between the mirrors ($159 \mu\text{m}$) and their radius of curvature (5 cm) yield a waist radius of the cavity mode of $w_{\text{cav}} = 23 \mu\text{m}$ and result in a mode volume of about $10^5 \times \lambda^3$. The mirrors are glued onto shear piezoelectric actuators (PZTs) for tuning the cavity length and thereby the cavity resonance frequency over 1.5 free spectral ranges.

The cavity is assembled on a specially designed cavity holder, which rests inside the glass cell on a short bellows, see figure 4. It is connected via a cardan joint to a 3D-positioner, consisting of an XY -manipulator (Thermionic Northwest, XY-B450/T275-1.39) and a Z -feedthrough (Thermionics Northwest, FLMM133). This combination allows us to adjust the cavity position with micrometre precision relative to the dipole trap axis. In order to locate the cavity mode along the dipole trap axis, we transport around 40 atoms having a broad position distribution along the dipole trap axis towards the cavity mode by a distance corresponding to an initial guess of the separation between the MOT and the cavity mode. In the cavity mode, we induce loss of atoms by heating them with the intracavity lock laser. Taking CCD pictures initially and after transporting back the atoms, we observe the position where atoms have been heated out. By tilting the dipole trap transverse to its axis, and looking for maximum atom loss, we can also locate the centre of the cavity mode along the x -axis.

2.2.1. Atom–light coupling. Due to a slight birefringence of our cavity mirrors, the resonances show a polarization splitting of several linewidths. The cavity therefore supports linear polarization modes only. For π -transitions from $F = 4$ to $F' = 5$ and for our parameters, the

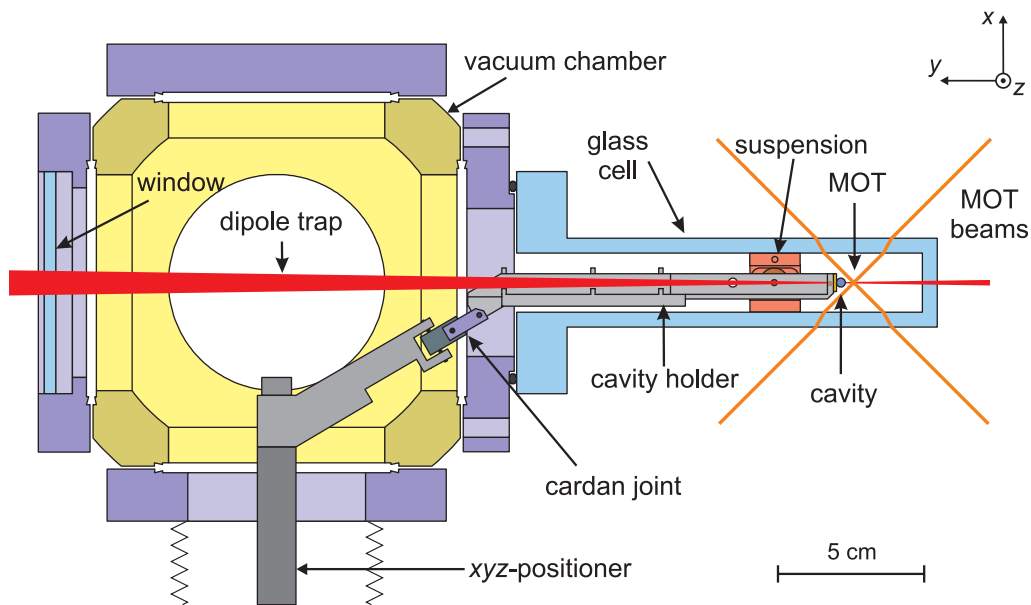


Figure 4. Cavity holder in the vacuum setup (top view). The adjustable holder is used for aligning the cavity position in the glass cell relative to the MOT. The resonator is placed about 4.6 mm away from the position of the MOT.

calculated coupling strength $g/2\pi$ ranges from 8 to 13 MHz for different m_F states. These values have to be compared to the dissipation rates of the coupled atom–cavity system. The field of the cavity decays at a rate of $\kappa/2\pi \approx 0.4$ MHz, and the atomic dipole decay rate of a caesium atom is $\gamma/2\pi = 2.6$ MHz. Since the condition $g \gg (\gamma, \kappa)$ is satisfied, the system operates in the *strong coupling regime*. The single atom cooperativity parameter $C_1 = g^2/(2\kappa\gamma)$, quantifying the coherent energy exchange versus dissipation rates, is expected to be in the order of 100.

2.2.2. Dissipation mechanisms. The ratio κ/γ determines the predominant dissipation mechanism, important for the extraction of information on the interaction between an atom and the cavity. In the optical domain often $\kappa \gtrsim \gamma$ [6]–[8] and the excitation of the coupled atom–cavity system predominantly decays via the cavity transmission. However, in our case κ has been made very small in order to achieve a high C_1 . Thus, for our value of $\kappa/\gamma = 0.15$, the excitation of the atom–cavity system decays rather by spontaneous emission of the atom than by the decay of the cavity field. We exploit this fact by using a spontaneous hyperfine changing Raman transition and by measuring the final internal atomic state. Such a change in the internal state can be induced by as few as one to two spontaneously scattered photons on average. An atom–cavity interaction can thus be detected even at very short interaction times, low probe light intensities, and at large laser-atom detunings by taking ensemble averages. In addition, the detection efficiency of the atomic state is close to unity in our case, by far exceeding our photon detection efficiency of only a few per cent.

2.2.3. Stabilization of the cavity. Cavity quantum electrodynamics (QED) experiments require precise control of the resonance frequency of the cavity relative to the atomic transition frequency. In order to keep the cavity resonance frequency stable within its linewidth, the cavity

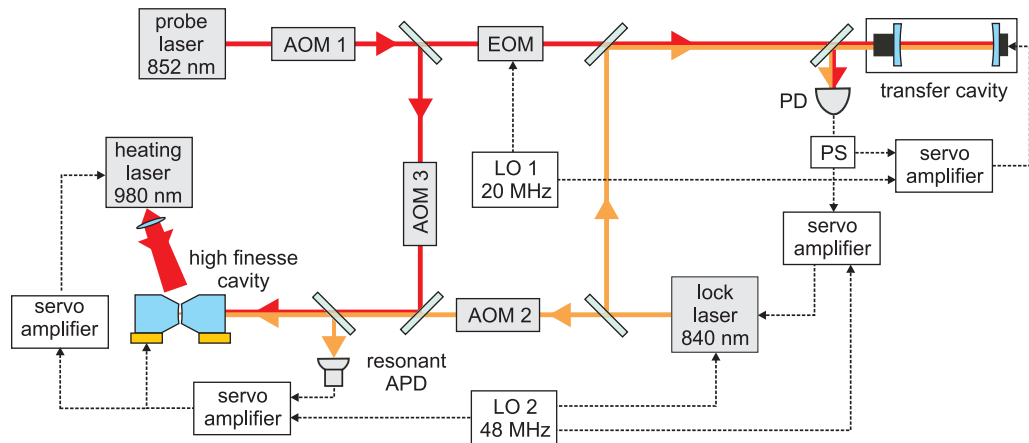


Figure 5. Frequency stabilization of the high-finesse cavity. Using the transfer cavity and the lock laser, the stability of the probe laser, which is stabilized to a caesium polarization spectroscopy, is transferred to the high-finesse cavity. AOM, acousto-optic modulator; EOM, electro-optic modulator; PD, photodiode; APD, avalanche photodiode; LO, local oscillator; PS, RF power splitter. The three servo loops are based on the PDH method.

length must be controlled to better than $\delta L \leq \lambda/(2\mathcal{F}) = 0.4 \text{ pm}$ in our case. During the entire experimental procedure it is therefore necessary to actively stabilize the cavity length against acoustic vibrations and thermal drifts. There are two major experimental issues to be considered: firstly, there is only marginal vibration isolation provided by the bellows (see section 2.2). Secondly, switching of the laser beams of the dipole trap causes thermal expansion of the cavity mirror assembly due to residual absorption. As a consequence, the unstabilized cavity resonance frequency drifts with an initial rate of about 2×10^5 linewidths per second within the first 300 ms after the dipole trap has been switched on. The corresponding servo loop therefore uses optimizations such as a double integrator and a notch filter compensating a mechanical resonance of the PZTs, and has a bandwidth of about 10 kHz.

We use an auxiliary far blue-detuned laser (‘lock laser’) at 840 nm for frequency stabilization. We thus suppress excitation of an atom by the intracavity lock laser field. Due to resonant enhancement, the injected lock laser power of $0.4 \mu\text{W}$ also creates a blue-detuned standing wave dipole potential with a height of about 0.3 mK and a maximum scattering rate of 40 s^{-1} .

Our locking scheme for the stabilization of the high-finesse cavity is similar to the one presented in [13]. Its main elements are schematically depicted in figure 5. Because of the absence of easily accessible atomic frequency references at $\lambda = 840 \text{ nm}$, the lock laser itself is stabilized onto an auxiliary cavity, which transfers the frequency stability of the probe laser to the lock laser. The error signals for all servo loops are based on the Pound–Drever–Hall (PDH) method [14]. The AOMs (AOMs 1–3 in figure 5) allow independent control of the probe-cavity detuning and probe-atom detuning within a range of $\pm 100 \text{ MHz}$.

Although the cavity resonance at 840 nm is stabilized onto the lock laser, we still observe drifts of the cavity resonance frequency at 852 nm with respect to the probe laser frequency on a timescale of several seconds. This residual frequency deviation is caused by different

temperature dependencies of the effective penetration depths into the mirror coatings for the two wavelengths. In order to compensate for this differential drift, we scan the cavity resonance over the probe laser frequency using AOM 2 and record a transmission spectrum of the cavity. Then, we determine the AOM control voltage which corresponds to the maximum transmission of the probe laser, and use this value in the following experimental cycle.

In order to compensate for large changes of the cavity length caused by long-term temperature variations exceeding the tuning range of the piezoelectric actuators, we heat the cavity using a multimode ‘heating laser’ at 980 nm and a power of up to 400 mW. Since we cannot directly measure the temperature of the cavity mirrors, we use the voltage applied to the piezoelectric actuators as an error signal. This signal is fed back onto the power of the heating laser in a slow servo loop, thus keeping the PZT offset voltage close to zero.

2.2.4. Detection of the cavity transmission. Both the lock laser and the probe laser beams share the same transverse mode profile. For the effect of the different longitudinal modes, see section 3.1.2 and figure 7. Since information about the atom–light interaction is only contained in the probe beam transmission, we separate them at the output of the cavity by a diffraction grating. For the detection of the probe beam transmission, we use a fibre-coupled single photon counting module (SPCM). It has a total measured quantum efficiency of about 30% and a dark count rate of 500 counts s⁻¹. The detection efficiency, i.e. the power detected by the SPCM divided by the power of the probe beam directly at the output of the cavity, is approximately 9%, including the diffraction efficiency of the grating, transmission of an interference filter, the losses on the remaining optics, and the quantum efficiency of the SPCM. In addition, since the light is partially absorbed and scattered by the cavity mirrors, the total efficiency for detection of intracavity photons is further reduced by a factor of $T/[2(T + A)]$ to about 2%.

3. Strong coupling of a single atom to the resonator mode

In order to characterize the interaction between atoms and the field mode, we have first carried out experiments with single atoms. We always tune the cavity into resonance with the probe laser, i.e. $\Delta_c = \Delta_p$, where $\Delta_c = \omega_c - \omega_a$ and $\Delta_p = \omega_p - \omega_a$. Here, ω_p , ω_c and ω_a are the angular frequencies of the probe laser, the cavity resonance and the ac-Stark shifted atomic $|F' = 4\rangle \rightarrow |F' = 5\rangle$ transition, respectively. The spatial profile of the coupling strength g as well as the spatial distribution of the probe laser field inside the cavity are defined by the TEM₀₀ cavity mode. Upon the insertion of a single atom into the resonator mode, the initially high transmission of a resonant probe laser drops due to the interaction-induced normal mode splitting.

3.1. Coupling to the centre of the mode

In order to demonstrate the coupling of a single atom to the cavity centre, we monitor the transmission of the probe laser beam while inserting the atom. Figure 6 presents an example of a single experimental cycle. At time $t = 0$, the SPCM is switched on. The background signal of about 10³ counts s⁻¹ corresponds to the dark counts and the stray light detected by the SPCM. The cavity and the probe laser are blue-detuned by $\Delta_c/2\pi \approx 24$ MHz. There exists theoretical work which indicates cooling in this regime [15]. However, we found this value empirically by observing an increased lifetime of the atoms inside the cavity.

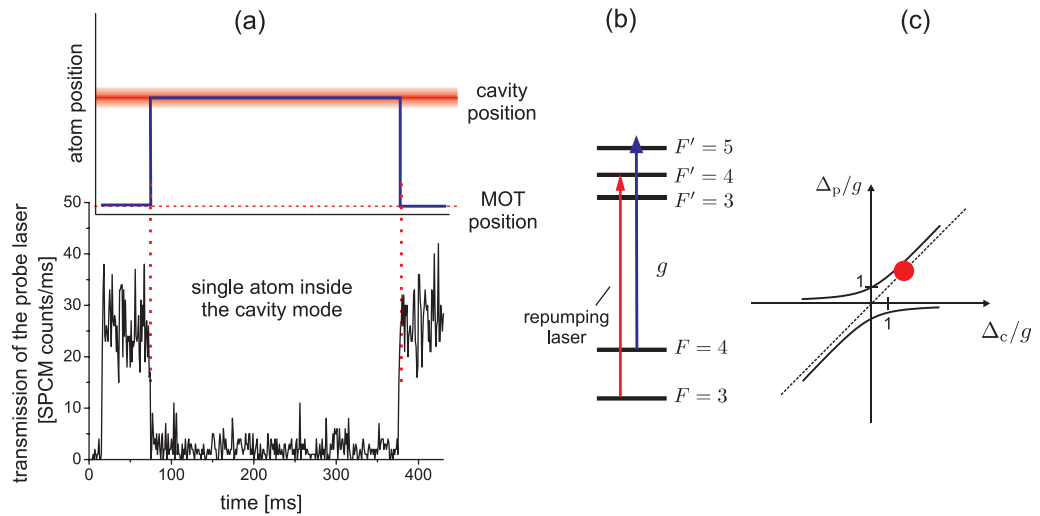


Figure 6. (a) Transmission signal versus time obtained in a single experimental run showing the case of continuous strong coupling. Upon placement of a single atom into the cavity mode, the transmission drops to 5% of its value for the empty cavity. After continuously observing the atom for 300 ms inside the cavity, it is transported back to the position of the MOT. (b) In this measurement, the cavity resonance is blue-detuned to the $|F = 4\rangle \rightarrow |F' = 5\rangle$ transition by $\Delta_c/2\pi \approx 24$ MHz. (c) Schematic illustration of the energies of the coupled atom–cavity states (solid lines) and the empty cavity state (dashed line). Our detunings Δ_c and Δ_p are shown as a red circle.

The probe laser beam is switched on at $t = 14$ ms resulting in a transmission count rate of 26×10^3 counts s^{-1} , corresponding to a mean intracavity photon number of about 0.1, indicating that we are in the regime of weak atomic excitation⁴. At $t = 70$ ms, we place an atom into the centre of the cavity mode, which causes the transmission of the probe laser to drop to 2×10^3 counts s^{-1} . Subtracting the background count rate, the transmission drops down to approximately 5% of its initial level. For our values of κ and γ and the chosen value of Δ_c , the observed drop in the probe transmission indicates strong coupling of the atom to the field of the resonator mode. During the entire experimental cycle, a repumping laser resonant with the $|F = 3\rangle \rightarrow |F' = 4\rangle$ transition is applied along the dipole trap axis. It transfers the atom back into the $F = 4$ state if it is off-resonantly pumped into the $F = 3$ state by the probe laser. The transmission remains at this level of 5% while the atom resides in the cavity until we transport the atom back to the position of the MOT. There we can take a second picture of the atom to not only verify its presence after the interaction with the cavity, but also to check that its position in the standing wave dipole trap has not changed, i.e. it has not been temporarily heated out of its potential well.

3.1.1. Model. In order to quantitatively analyse our measurements and to establish a relation between g and the observed average transmission, we model our physical system including a

⁴ At this intracavity photon number for an empty cavity, the scattering rate of an atom coupled to the cavity is much smaller than γ for any detuning Δ_c and any coupling strength g .

variation of g caused by the internal and external dynamics of the atom. For this purpose, we numerically solve the master equation of the coupled atom–cavity system [16]. All processes causing a variation of the coupling strength g are slow compared to the decay time $1/\kappa$ of the cavity field. Therefore, the cavity transmission at any moment is determined by the instantaneous coupling strength. Since g is time-dependent and the cavity transmission is a nonlinear function of g , we simulate the measured average transmission level by first calculating the transmission levels corresponding to all possible values of g , and then computing the weighted average over these levels.

The internal dynamics of the atom is caused by its continuous scattering of photons while coupled to the cavity mode, which causes changes in the Zeeman sublevel occupation. Since the atom is not optically pumped into a specific m_F sublevel of the ground state $F = 4$, we assume a homogeneous distribution over all these states and average over the transmissions corresponding to the different m_F states.

The external dynamics is given by the motion of the atom in the trapping potential. We assume a thermal Boltzmann energy distribution neglecting modifications due to cavity QED effects, the multi-level atomic structure and technical noise which could lead to a non-thermal energy distribution [15]. Since our integration time is much longer than the heating and cooling timescales, our model allows us to assign an effective temperature corresponding to the time-averaged energy $\langle E \rangle$ of the atom in the trap via $\langle E \rangle = 3k_B T$. We take into account the variation of g and the variation of the ac-Stark shift, due to the dipole trap and the lock laser, caused by the oscillatory motion. The depth of the dipole potential due to the intracavity photon number of the probe laser corresponding to the empty cavity ($n = 0.1$) is only about $30 \mu\text{K}$ at the centre of the cavity mode [17]. An atom coupled to the mode strongly reduces the photon number, which further decreases this potential to values much lower than the atomic temperature and all other trapping potentials. We therefore neglect the effect of this potential.

Along the x -axis, transverse to both the dipole trap and the cavity axis, the atom is weakly confined by the Gaussian profile of the dipole trap. Due to oscillations along this direction, the atom experiences a variation of the ac-Stark shift and the coupling strength g . Along the z -axis, the atom is well localized to several hundred nanometres by the lock laser standing wave with a potential height of $U/k_B \approx 0.3 \text{ mK}$. Along the dipole trap axis (y -axis) the variation of g is negligible and we consider the variation of the ac-Stark shift only.

We use the model temperature as a fit parameter in our numerical simulations and find that a temperature of about 0.17 mK reproduces our observed drop of the transmission to 5%. This result indicates a somewhat higher temperature than the typical 0.07 mK inside our dipole trap after molasses cooling possibly due to different cooling and heating mechanisms present inside the cavity.

3.1.2. Observation of trapping dynamics. In experimental records, we frequently observe strong variations of the transmission as shown in figure 7(a). We attribute these to hopping of atoms between different trapping sites along the cavity axis (z -axis): due to the dynamic equilibrium between cooling and heating processes in the cavity, the atom can be heated out of one node of the blue-detuned lock laser standing wave and subsequently be cooled into a different node. Since the lock and probe laser standing waves have different periodicities due to their different wavelengths, the coupling strength at potential minima of the lock laser standing wave changes from maximum to minimum over a length of $d_{\text{beat}}/2 = 15 \mu\text{m}$, as depicted in figure 7(b). Therefore, the hopping of atoms along the z -axis can result in sudden strong changes

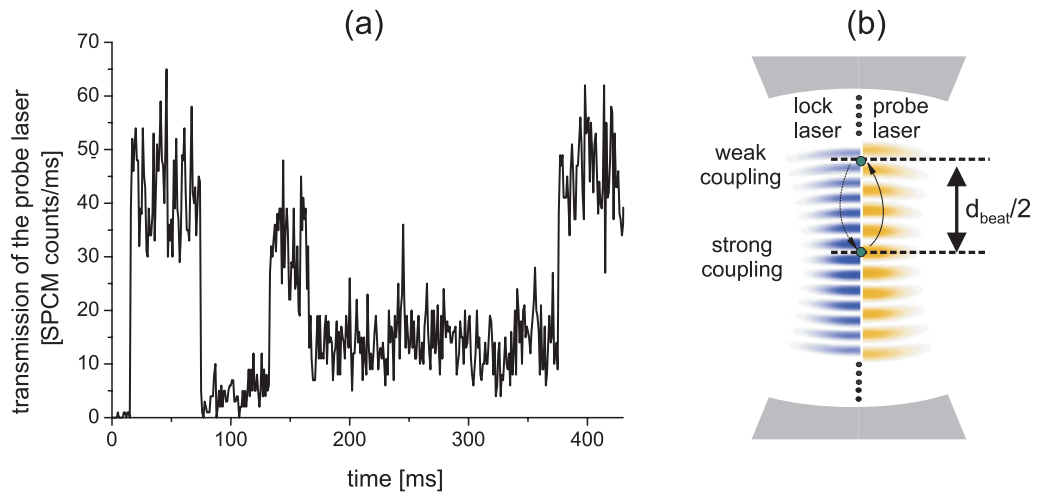


Figure 7. (a) Transmission signal of the probe laser beam through the cavity for the case of time-dependent coupling. (b) Due to jumps between different nodes of the repulsive lock laser standing wave, the coupling strength of the atom to the cavity changes.

of the atom–cavity coupling strength, leading to jumps of the transmission level. We observe that the rate of these transmission variations seems to depend critically on a complex interplay between lock and probe laser intensities, detuning and the initial insertion conditions. This phenomenon, however, is not yet fully understood and requires further investigation.

Note that the data presented in figure 6 have been selected for strongest coupling and no hopping. In the corresponding simulations, we have assumed the atom to reside at a potential minimum coinciding with a maximum of g .

3.2. Position-dependent coupling

Applications of cavity QED in quantum information experiments with a string of atoms usually require control of the coupling strengths for different atoms. This can be achieved e.g. by suitably positioning them inside the mode profile. In order to map out the spatial distribution of the coupling strength transverse to the cavity axis, we continuously observe the transmission while transporting a single atom slowly through the mode, similar to the experiments reported in [6, 8].

We first shuttle the atom to the edge of the mode $50 \mu\text{m}$ from the mode centre, where g is negligible. As depicted in figure 8, by slowly transporting the atom over $100 \mu\text{m}$ across the cavity mode within 150 ms, we observe a continuous variation of the transmission caused by a variation of g . After a waiting time the direction of the slow transport is reversed. For both transportation directions, the average transmission drops to about 20% of its maximum level in the centre of the cavity mode, and the shape of the transmission is almost identical.

The drop to about 20% is less than the reduction in the previous single-shot experiment. This is a result of averaging over 19 shots, selected only for the presence of the atom during the complete transportation in both directions, and of a larger blue detuning of $\Delta_c/2\pi \approx 44 \text{ MHz}$. Due to thermal oscillations along the z -axis inside the dipole trap, the atom enters the cavity field in different nodes of the lock laser standing wave, thus causing the coupling strength and

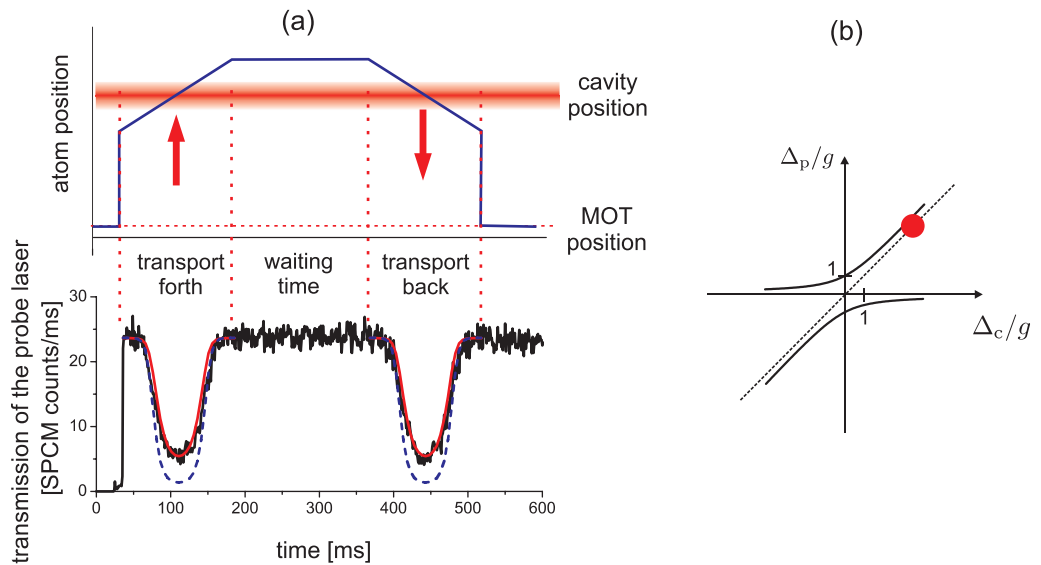


Figure 8. (a) Transmission of the probe laser beam as an atom is slowly swept back and forth across the cavity mode over a distance of $100 \mu\text{m}$ within 150 ms . The trace is an average over 19 experimental runs. The measured data are in good agreement with the numerical simulation (solid line in red). The probe laser is blue-detuned with respect to the $|F = 4\rangle \rightarrow |F' = 5\rangle$ atomic transition by $\Delta_c/2\pi \approx 44 \text{ MHz}$. The dashed blue line indicates the cavity transmission assuming no thermal motion and strongest coupling along the cavity axis. (b) Schematic illustration of the energies of the coupled atom–cavity states; our detunings Δ_c and Δ_p are shown as a red circle.

the reduction of the transmission to have different values for each transport through the cavity mode. We perform a numerical simulation for comparing our observations with the prediction of our simple model. With the temperature as a single fit parameter, our numerical simulations are in good agreement with the measured data by assuming a temperature of about 0.13 mK .

4. Coupling of one and two atoms

For N atoms simultaneously coupled to the cavity mode, the effective collective coupling strength g_N is expected to scale as $g\sqrt{N}$ for weak excitation, where g is the coupling strength of a single atom. In figure 9, we compare the cavity transmission when sweeping either one or two atoms slowly through the cavity mode. In the case of two atoms, their separation is below $1.5 \mu\text{m}$, which is small compared to the waist of the cavity mode. We therefore assume that the two atoms interact with the cavity mode simultaneously at the same position. The data in figure 9 are single experimental runs and are selected for strongest coupling along the z -axis, as discussed in the previous section. In the central region of the cavity, already a single atom almost completely blocks the transmission of the probe laser. However, at the outer regions of the cavity mode, two atoms cause a significantly stronger drop in transmission than a single atom.

In analogy to the previous section, we performed a numerical simulation, assuming that the intracavity temperature of the atoms is the same as in the experiment presented in figure 6.

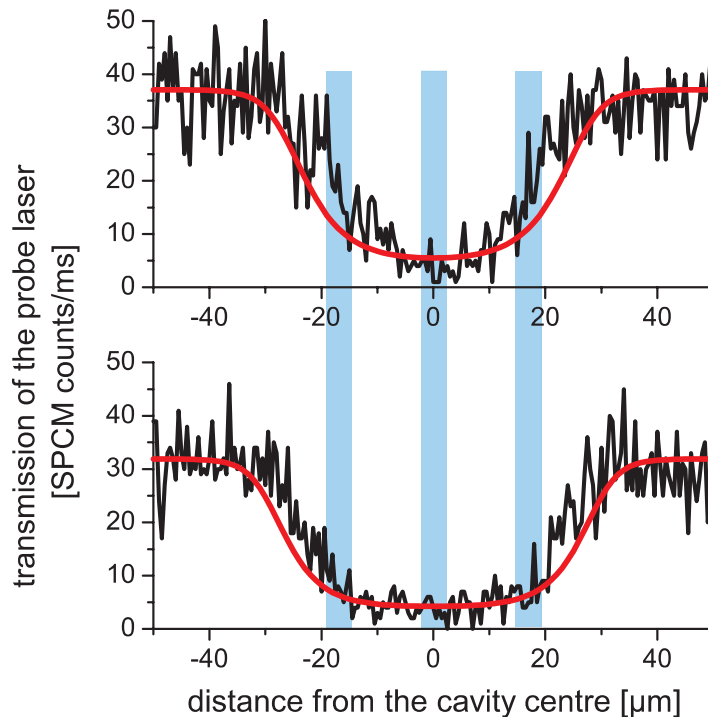


Figure 9. Transmission of the probe laser beam as a single atom (upper panel) and two atoms (lower panel) are swept across the cavity mode. For the latter case the width of the transmission dip is notably larger, indicating a stronger coupling strength. The probe laser is blue-detuned with respect to the $|F = 4\rangle \rightarrow |F' = 5\rangle$ atomic transition by $\Delta_c/2\pi \approx 24$ MHz. The measured data agrees reasonably well with the numerical simulation (solid red lines) for one and two atoms in the upper and lower graphs, respectively.

The case of two atoms is approximated here by a single atom coupled to the cavity with a strength $g \times \sqrt{2}$. The numerical simulation agrees well with the measured data for the central region of the cavity. In the outer regions, both measured transmission levels are slightly higher than the calculation. This deviation is to be expected, as our simple model assumes constant confinement of the atom by the blue-detuned lock-laser standing wave independent of the position along the dipole trap axis. However, this confining potential decreases towards the edge of the cavity mode, and at some point the atom is no longer confined by the lock laser standing wave. As a result, the atom oscillates freely along the z -axis and experiences on average a weaker coupling strength, thus increasing the transmission level.

5. Detection of the final atomic state

We now present a complementary method for extracting information about atom–cavity coupling which is based on the detection of the internal atomic state after an atom has interacted with the field of the resonator. In the microwave domain, this method is used in the cavity QED experiments of S Haroche, J-M Raimond and co-workers [18].

For this measurement, we prepare a single atom in the dipole trap in the hyperfine ground state $F = 4$ by illuminating it with the MOT repumping laser. We then transport the atom to the

cavity mode and subsequently inject the probe laser beam into the cavity. In this experiment, the cavity is blue-detuned by about 40 MHz from the $|F = 4\rangle \rightarrow |F' = 3\rangle$ transition and is red-detuned by 160 MHz from the $|F = 4\rangle \rightarrow |F' = 4\rangle$ transition. During the interaction time of 1 ms, the injected probe laser power corresponds to about 0.04 photons inside the cavity, much less than what was used in the previous experiments presented hereinbefore. The atom is pumped into the non-interacting $F = 3$ ground state with a probability proportional to the intracavity probe light intensity, after scattering a few photons only. We retrieve the atom from the cavity and subsequently detect its final state with an efficiency close to unity by applying a ‘push-out’ laser [19]. This laser is resonant with the $|F = 4\rangle \rightarrow |F' = 5\rangle$ transition and removes all the atoms in $F = 4$ from the trap. Subsequent transfer of the remaining atoms back to the MOT reveals the number of atoms in $F = 3$. In order to ensure the efficient operation of the ‘push-out’ laser, we reduce the depth of the dipole trap after transporting atoms back to the MOT position, which limits the overall survival probability of the atoms in $F = 3$ to $77_{-9}^{+7}\%$.

For each position of the atom inside the cavity mode, we take an ensemble average of about 40 repetitions. By varying the atomic position across the cavity mode, we map out the optical pumping rate due to the probe laser beam inside the cavity, see figure 10(a). We observe a peak in population transfer corresponding to the transverse cavity mode profile with a maximum transfer efficiency of about 60%. In this experiment, an atom interacts dispersively with the cavity field and has only a small effect on the intracavity photon number. Therefore, this photon number still weakly depends on the distance of the atom from the cavity mode centre and on the initial m_F state of the atom. As an example, figure 10(c) shows the normalized photon number as a function of atomic distance from the cavity centre in the case of an atom occupying the state $|F = 4, m_F = 1\rangle$. The resulting probe laser intensity, shown in figure 10(d), is slightly broader than the Gaussian intensity profile in the absence of an atom. Compared to figure 10(d), the transfer efficiency curve is further broadened due to the nonlinear dependence of the transfer efficiency on the probe light intensity. This dependence, shown in figure 10(e), is modelled for each initial m_F state by performing Monte-Carlo simulations and taking thermal motion into account, as was described in section 3.1. We divide the holding time of an atom inside the cavity into 10 μs intervals, short compared to the average scattering rate. In each of these intervals, the atom is assumed to be either excited with a probability determined by the local probe laser intensity and the corresponding Clebsch–Gordan coefficient and then to decay to the hyperfine state $F = 4$ or $F = 3$ with the corresponding branching ratios; or it remains in the state $F = 4$. The result of this simulation for the initial state $|F = 4, m_F = 1\rangle$ is shown in figure 10(e). It is used for computing the spatial variation of the population transfer from the probe intensity distribution of figure 10(d). We again assume a homogeneous distribution over different m_F states and average the population transfer over these states. Since the simulation shows only a very slight dependence on the temperature, we use the intracavity photon number as a single fit parameter. The resulting photon number of 0.02 equals 60% of the expected photon number estimated from the transmission. We attribute this deviation to systematic uncertainties of our model and inaccuracies of our measurement. The theoretical curve in figure 10(a) is obtained by normalizing the simulated averaged population transfer to the survival probability of 77% and fits well to the observed data.

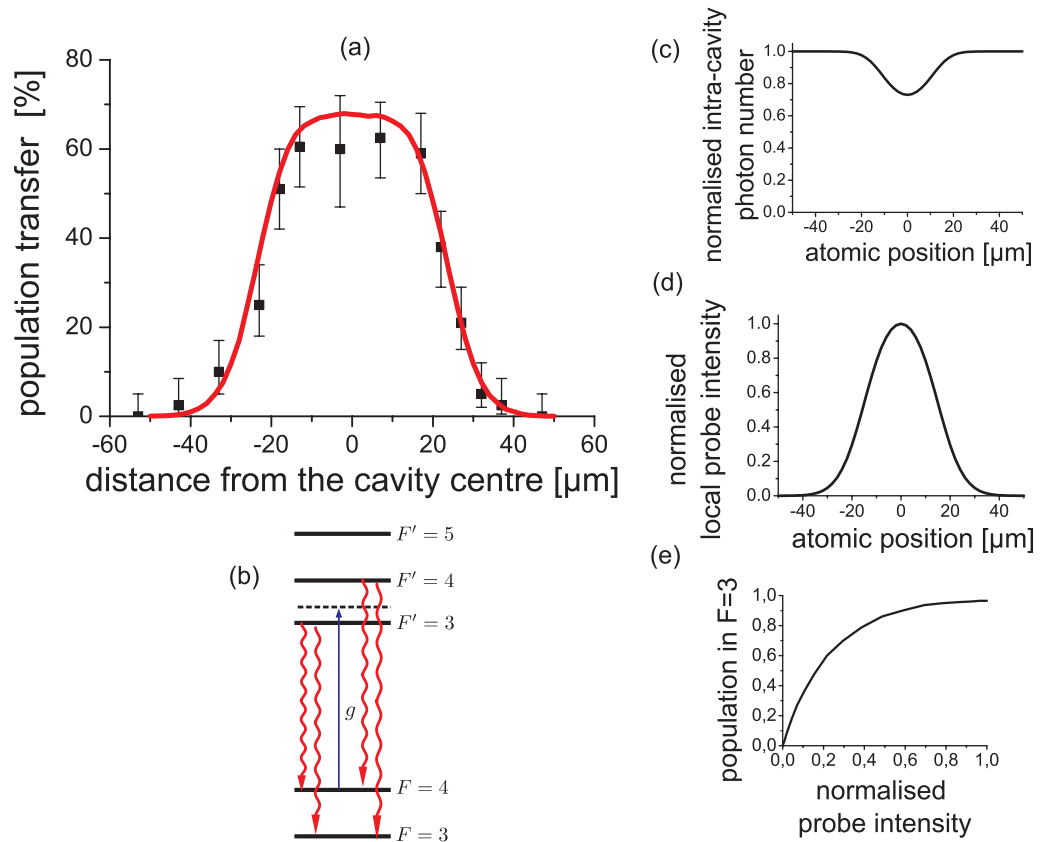


Figure 10. (a) Measurement of the final state of the atom after it has interacted with the field of the cavity mode. Each point is the result of about 40 experimental runs with a single atom. (b) The probe laser is blue-detuned from the $|F = 4\rangle \rightarrow |F' = 3\rangle$ transition by 40 MHz and is red-detuned from the $|F = 4\rangle \rightarrow |F' = 4\rangle$ transition by 160 MHz. Model for an atom in the state $|F = 4, m_F = 1\rangle$: (c) intracavity photon number and (d) local probe laser intensity as a function of the atomic position and (e) pumping efficiency as a function of local probe laser intensity. The solid red line in (a) is then obtained by taking the composition of (d) and (e), performing these calculations for each state $|F = 4, m_F\rangle$, and averaging subsequently.

6. Summary and outlook

We have presented an apparatus to strongly couple a well-controlled number of atoms to a high-finesse optical resonator. Observation of the cavity transmission could allow us to detect and examine the motional dynamics of one and two atoms in the cavity [15, 20]. The observed position-dependent variation of the interaction strength, together with an improved localization of atoms inside the cavity, offers a tool to fully control the atom–cavity coupling strength. Measuring the final hyperfine state of the atom allows us to detect the interaction with the cavity, while heating effects are strongly suppressed due to the short interaction time and small probe laser power. Using this method, the next step is to reveal the coherent nature of the atom–cavity interaction by observing the vacuum Rabi splitting [21]–[23] once we have established a better control over the coupling strength. We finally aim at the generation of entanglement between

two atoms and at the creation of multi-atom correlated quantum states utilizing our ability to selectively initialize and manipulate the internal state of individual atoms [1].

Acknowledgments

We thank A Stiebeiner for her help with the cavity stabilization. This work in early stages was supported by the Deutsche Forschungsgemeinschaft within the Schwerpunkt ‘Quanten-Informationsverarbeitung’ as well as by the European Commission within the project ‘QGATES’. In the final stage this work was supported by the European Commission within the project ‘SCALA’. SR acknowledges support from the ‘Deutsche Telekom Stiftung’ and TK acknowledges support from the ‘Studienstiftung des deutschen Volkes’ and from the ‘Bonn–Cologne Graduate School of Physics and Astronomy’.

References

- [1] Schrader D, Dotsenko I, Khudaverdyan M, Miroshnychenko Y, Rauschenbeutel A and Meschede D 2004 *Phys. Rev. Lett.* **93** 150501
- [2] Nielsen M A and Chuang I L 2000 *Quantum Computation and Quantum Information* (Cambridge: Cambridge University Press)
- [3] Pellizzari T, Gardiner S A, Cirac J I and Zoller P 1995 *Phys. Rev. Lett.* **75** 3788
- [4] Zheng S B and Guo G C 2003 *Phys. Rev. Lett.* **85** 2392
- [5] Osnaghi S, Bertet P, Auffeves A, Maioli P, Brune M, Raimond J M and Haroche S 2001 *Phys. Rev. Lett.* **87** 037902
- [6] Nussmann S, Hijlkema M, Weber B, Rohde F, Rempe G and Kuhn A 2005 *Phys. Rev. Lett.* **95** 173602
- [7] McKeever J, Buck J R, Boozer A D, Kuzmich A, Nägerl H C, Stamper-Kurn D M and Kimble H J 2003 *Phys. Rev. Lett.* **90** 133602
- [8] Fortier K M, Kim S J, Gibbons M J, Ahmadi P and Chapman M S 2007 *Phys. Rev. Lett.* **98** 233601
- [9] Puppe T, Schuster I, Grothe A, Kubanek A, Murr K, Pinkse P W H and Rempe G 2007 *Phys. Rev. Lett.* **99** 013002
- [10] Förster L, Alt W, Dotsenko I, Khudaverdyan M, Meschede D, Miroshnychenko Y, Reick S and Rauschenbeutel A 2006 *New J. Phys.* **8** 259
- [11] Alt W, Schrader D, Kuhr S, Müller M, Gomer V and Meschede D 2003 *Phys. Rev. A* **67** 033403
- [12] Dotsenko I, Alt W, Khudaverdyan M, Kuhr S, Meschede D, Miroshnychenko Y, Schrader D and Rauschenbeutel A 2005 *Phys. Rev. Lett.* **95** 033002
- [13] Mabuchi H, Ye J and Kimble H J 1999 *Appl. Phys. B* **68** 1095
- [14] Drever R and Hall J 1983 *Appl. Phys. B* **31** 97
- [15] Domokos P and Ritsch H 2003 *J. Opt. Soc. Am. B* **20** 1098
- [16] Carmichael H 1993 *An Open Systems Approach to Quantum Optics* (Berlin: Springer)
- [17] Brune M, Nussenzweig P, Schmidt-Kaler F, Bernardot F, Maali A, Raimond J M and Haroche S 1994 *Phys. Rev. Lett.* **72** 3339
- [18] Gleyzes S, Kuhr S, Guerlin C, Bernu J, Deleglise S, Hoff U B, Brune M, Raimond J M and Haroche S 2007 *Nature* **446** 297
- [19] Kuhr S, Alt W, Schrader D, Dotsenko I, Miroshnychenko Y, Rosenfeld W, Khudaverdyan M, Gomer V, Rauschenbeutel A and Meschede D 2003 *Phys. Rev. Lett.* **91** 213002
- [20] Asbóth J K, Domokos P, Ritsch H and Vukics A 2005 *Phys. Rev. A* **72** 053417
- [21] Sanchez-Mondragon J J, Narozhny N B and Eberly J H 1983 *Phys. Rev. Lett.* **51** 55
- [22] Boca A, Miller R, Birnbaum K M, Boozer A D, McKeever J and Kimble H J 2004 *Phys. Rev. Lett.* **93** 233603
- [23] Maunz H J, Puppe T, Schuster I, Syassen N, Pinkse P W H and Rempe G 2005 *Phys. Rev. Lett.* **94** 033002